Materials Research. 2023; 26:e20230302
DOI: https://doi.org/10.1590/1980-5373-MR-2023-0302

A Modified Description with Variable Parameters of Flow Behaviors for Ni-38Cr-3.8Al Alloy

Guo-zheng Quan[a]*, Sheng Lei[a], Yu Zhang[a], Wei-Wei Dai[b], Qian Jiang[b], Li-he Jiang[b]

[a]Chongqing University, School of Material Science and Engineering, Chongqing Key Laboratory of Advanced Mold Intelligent Manufacturing, 400044, Chongqing, China.
[b]COSCO Shipping Marine Equipment & Spares (Nanjing) Co., Ltd., Jiangsu Advanced Manufacturing Engineering Technology Research Center for Marine Power System Parts, 211121, Nanjing, China.

Received: July 02, 2023; Revised: October 17, 2023; Accepted: October 31, 2023

Nickel-based alloys containing high amount of Cr are desirable materials for the production of critical components that operate under high temperature and severe corrosion conditions. The description of flow behaviors for these alloys is key to designing the hot formation process for achieving the excellent mechanical properties of components. This work aims to study the flow behaviors of Ni-38Cr-3.8Al alloy during thermal deformation. A series of isothermal compression experiments were carried out at temperatures of 1148 K, 1223 K, 1298 K, 1373 K, 1448 K and 1523 K, and strain rates of 0.01 s^{-1}, 0.1 s^{-1}, 1 s^{-1} and 10 s^{-1}. Results show that the obtained true stress-strain curves exhibit the softening characteristics of dynamic recrystallization (DRX) and dynamic recovery (DRV). The flow stress decreases with temperature increasing and strain rate decreasing. To further quantitatively describe the flow behaviors, an improved segmented Arrhenius constitutive equation was developed according to the softening characteristics under different temperatures. In these equations, the variable coefficients, including activation energy Q and material constants (structure factor A, stress exponent n, stress parameters α), were fitted as the polynomial functions of true strain. Furthermore, a typical Arrhenius constitutive equation was also solved. The comparisons between experimental stress and predicted results obtained from the typical and improved constitutive equations were conducted, and the correlation coefficient (R) and average absolute relative error ($AARE$) were calculated as 0.932, 15.83%, and 0.9963, 5.61%, respectively. It suggests that the improved constitutive equation can adeptly describe the flow behaviors of Ni-38Cr-3.8Al alloy.

Keywords: *Nickel-based superalloy, Flow behaviors, Activation energy, Constitutive equation.*

1. Introduction

Nickel-based superalloys are often the preferred material for high-temperature structural applications, particularly in situations where the risk of degradation due to oxidation and corrosion is severe. Numerous researches have demonstrated that the presence of a higher concentration of chromium (Cr) within the nickel (Ni) matrix effectively mitigates the risk of oxidation and corrosion, as chromium readily undergoes substantial dissolution[1]. Due to the discontinuous precipitation reaction (DP), Ni-Cr binary alloys containing high Cr concentration exhibit a lamellar microstructure composed of the γ phase with face-centered cubic (fcc) structure and the α phase with body-centered cubic (bcc) structure. Especially, the lamellar structure formed by the DP has significant influence on the microstructure and mechanical properties of these alloys. Moreover, it is reported that an addition of Al to these Ni-Cr alloys leads to an excess supersaturation of Cr by the precipitation of the γ' (Ni_3Al) phase, which accelerates the DP reaction rate in Ni-Cr-Al ternary alloys[2]. Ni-38Cr-3.8Al alloy, a typical Ni-Cr-Al ternary alloy, possesses high strength and hardness, excellent creep resistance and corrosion resistance, which has the fine lamellar structure due to DP reaction[3]. As a new generation of heat-resistant alloy with optimization of Cr and Al concentrations, Ni-38Cr-3.8Al alloy has been applied in engine components superior to the traditional Ni80A superalloy[4,5]. These components are usually achieved by a thermal forming process, such as forging, extrusion, electric upsetting, etc. The mechanical properties of the components after a thermal deformation depend on the microstructural characteristics that are strongly related to the forming parameters including strain, strain rate and temperature. It is essential to design and optimize the processing parameters to obtain the desired mechanical properties of a component via the finite element method. Therefore, developing a high-accuracy characterization of flow behaviors, which contributes to the accuracy of numerical simulation, is a crucial issue for process design and optimization.

A constitutive model always takes into account the dependence of stress on deformation parameters, and has been widely employed to characterize the flow behaviors of metal materials. Sellars and McTegart[6] first proposed an Arrhenius-type constitutive equation, which described the

*e-mail: quangz3000@sina.com

relationships between flow stress, strain rate and temperature by the sine-hyperbolic laws. In the following, Song et al.[7], Cingara and McQueen[8] solved the Arrhenius-type constitutive equation at peak stress to obtain the activation energy Q and stress exponent n of Mg-6Zn-0.5Mn-0.3Cu-0.02Zr alloy and 300 austenitic steels respectively. Lin et al.[9] proposed a modified Arrhenius-type equation considering strain compensation to comprehensively describe the influence of the three processing parameters (including temperature, strain rate and strain) on the flow behaviors of 42CrMo steel. Wherein the variable coefficients including activation energy Q and material constants (structure factor A, stress exponent n, stress parameters α) were fitted as the polynomial functions of true strain. In the same way, large number of scholars such as Nie et al.[10], Quan et al.[11], Yi et al.[12] and others solved the modified Arrhenius-type constitutive equation to characterize the flow behaviors of Mg-9Gd-4Y-2Zn-0.5Zr, AZ80, TC21 alloys and so on, respectively. Moreover, it is noted that the three deformation mechanisms including work hardening (WH), DRV softening, and DRX softening coexist during the hot deformation process. According to the different dominant softening mechanisms, the flow curves can be divided into two types involving DRX-type and DRV-type curves. When the two kinds of curves simultaneously exist in the hot deformation flow curves of materials, the values distributions of stress in a certain are relatively discrete. The accumulated errors in the solving process of the Arrhenius-type constitutive equation would ultimately lead to a large deviation between the predicted value and the experimental value, and reduce the prediction accuracy of the model[13]. So far, for the new generation nickel-based superalloy, Ni-38Cr-3.8Al alloy, it is urgent to develop an improved constitutive model to accurately describe its flow behaviors. This significantly contributes to the high accuracy simulation analysis for the thermal forming process of Ni-38Cr-3.8Al alloy.

This work aims to investigate the flow behaviors of Ni-38Cr-3.8Al alloy through the improved Arrhenius-type equation. A series of isothermal compression experiments were conducted under a wide deformation temperature range of 1148~1523 K and a wide strain rate range of 0.01~10 s^{-1}. The characteristics of flow behaviors were analyzed from the obtained stress-strain curves. The typical and improved constitutive equations were solved based on the stress-strain data. The comparisons between experimental results and predicted results obtained from the modified of typical and improved constitutive equations were conducted, and the R and $AARE$ were calculated as 0.932, 15.83% and 0.9963, 5.61%, respectively.

2. Materials and Methods

The material used in this investigation is Ni-38Cr-3.8Al alloy, and its chemical compositions are (wt.%) Cr 38, Al 3.8, C 0.01, B 0.003, Mg 0.003, Ni (balance). Twenty-four standard cylindrical specimens with a diameter of 10 mm and a height of 12 mm were machined from the hot-rolled bar for the following isothermal compression experiments. The isothermal compression experiments were carried out under the temperature range of 1148~1523 K and the strain rate range of 0.01~10 s^{-1} on a computer-controlled, servo-hydraulic Gleeble-3500 thermo-mechanical simulator. The detailed procedures of isothermal compression experiments are illustrated in Figure 1. It's noteworthy that the friction between the specimen and the anvil may have a significant effect on the true stress. Tantalum sheets, possessing lower surface roughness and adhesion, are often used as molds or as an interlayer between specimen and anvils during the hot compression process to reduce the friction and promote the uniform deformation of the specimen. Here, tantalum sheets were placed on both ends of the specimen before the experiment. Firstly, the specimen was heated by AC current at a heating rate of 10 K/s until the temperature reached to a setting value. Subsequently, the specimen was held at this temperature for 180 s to decrease the material anisotropy. Following that, the heated specimen was compressed up to the height reduction of 60%, i.e. the true strain of 0.916, with a specified strain rate. After the compression, the compressed specimen was immediately cooled by water quenching to retain the elevated temperature microstructures. During the isothermal compression processes, the nominal stress-strain data were collected by a force conductor and a displacement conductor. The true stress and true strain were derived from the nominal data according to the following formulas: $\sigma_T = \sigma_N(1-\varepsilon_N)$, $\varepsilon_T = \ln(1-\varepsilon_N)$, where σ_T is true stress, σ_N is nominal stress, ε_T is true strain and ε_N is nominal strain.

3. Results and Discussion

3.1. Description of flow behaviors from stress-strain curves

The true stress-strain curves of Ni-38Cr-3.8Al alloy obtained from isothermal compression experiments are shown in Figure 2. Figure 3 illustrates the typical flow curves for cold and hot deformation processes. It can be seen from Figure 3 that in the cold deformation process, the flow stress increases sharply with the increase of true strain, and work hardening is the predominant deformation mechanism. For the hot deformation process, it is noted that the three deformation mechanisms including WH, DRV softening, and DRX softening coexist. According to the different dominant softening mechanisms, the flow curves can be divided into two types involving DRX-type and DRV-type curves. On the basis of Figure 3, it is concluded from Figure 2 that the conditions of the true stress-strain curves exhibit DRX-type

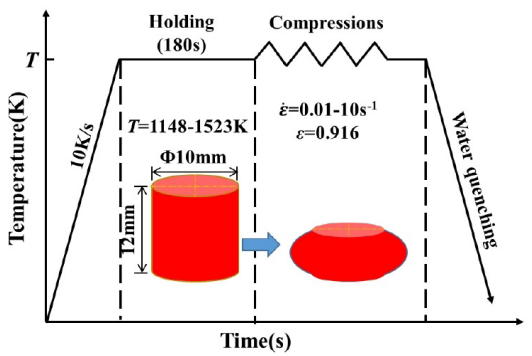

Figure 1. Procedures of isothermal compression experiment.

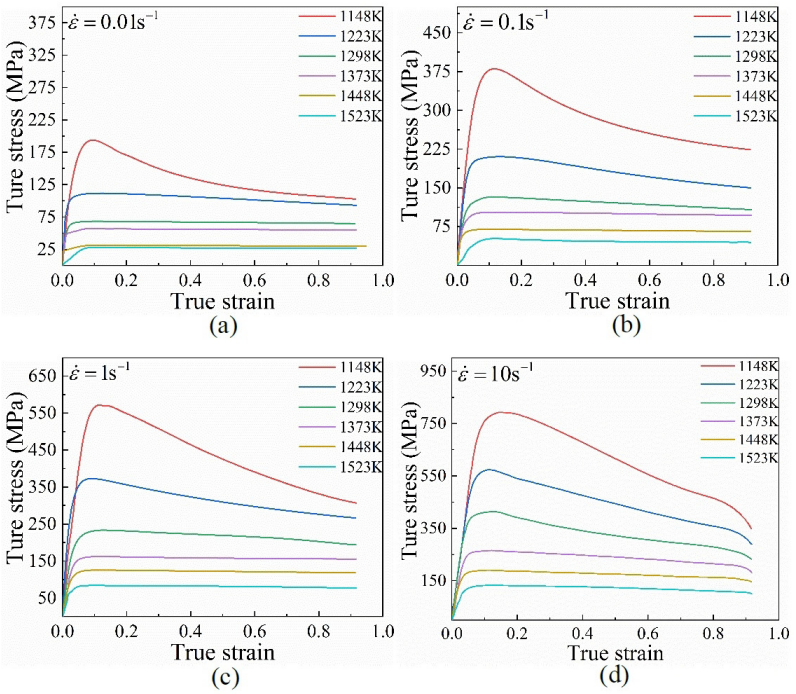

Figure 2. True strain-stress curves for Ni-38Cr-3.8Al alloy under different deformation temperatures with strain rates of: (a) 0.01 s^{-1}; (b) 0.1 s^{-1}; (c) 1 s^{-1}; (d) 10 s^{-1}.

characteristics as follows: at T=1148~1298 K, all strain rates. The evolution of flow stress varying with true strain can be divided into three stages. At the initial stage, the flow stress increases sharply with true strain increasing. This is because WH caused by the multiplication and entanglement of dislocations, and DRV caused by dislocations migrating and climbing is insufficient to resist it. In the second stage, with the increase of true strain, the flow stress increases gradually to a peak value, while the slope of the curve decreases. This can be attributed to the fact that when the dislocations reach a critical value, the DRX mechanism occurs, resulting in the annihilation of dislocations. While the WH is still the predominant deformation mechanism. As the true strain increases continuously, DRX softening behavior becomes stronger and exceeds DRV softening in a moment. Under the comprehensive softening actions of DRV and DRX, the action of WH is gradually counteracted. When the flow stress increases to a peak value, the first balance between WH and softening behaviors arrives. In the third stage, the flow stress begins to decrease gradually with increasing strain under the dominant role of DRX softening. In this stage, the softening rate gets higher until it reaches the maximum value. As the strain increases continually, the softening rate of DRX starts to decrease, while the effect of WH is highlighted. With that, the flow stress tends to a steady state under the second dynamic balance between WH and DRX softening behaviors. At T=1298~1523 K, all strain rates, the true stress-strain curves show DRV-type characteristics. Different from the DRX-type characteristics, there is no significant peak stress appears on the curves. When the flow stress increases to a certain value, with increasing of true strain, the flow stress almost keeps the same value under the dynamic equilibration between WH and

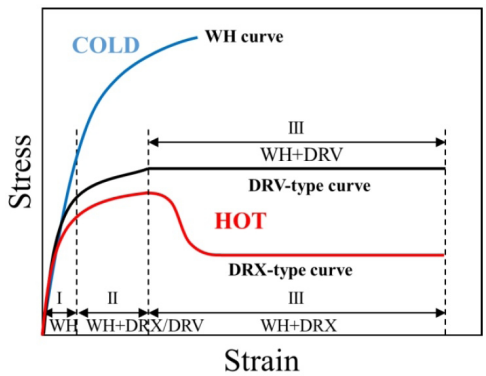

Figure 3. Typical flow curves during cold and hot deformation processes.

DRV-predominant softening behaviors. From Figure 2, it also can be seen that the flow stress level was mightily determined by temperature and strain rate. The flow stress level increases with the decrease of temperature and the increase of strain rate. This is due to the fact that higher temperature can provide more activation energy for the nucleation of DRX and DRV grains, and improve the grain boundary migration rate. In addition, at lower strain rate, there is adequate time for the annihilation of dislocations in the deformed specimens[14].

3.2. Solving process of typical Arrhenius-type constitutive equation

In this work, the hyperbolic-sine Arrhenius-type constitutive equation was employed to further describe the flow behaviors

under various deformation parameters. In this equation, the relationships between peak flow stress(σ_P), strain rate and temperature can be described as Equation 1.

$$\dot{\varepsilon} = A\left[\sinh\left(\alpha\sigma_P\right)\right]^n \exp\left[-Q/\left(RT\right)\right] \tag{1}$$

where $\dot{\varepsilon}$ is strain rate (s^{-1}); σ is the flow stress (MPa); A is structure factor; n is stress exponent; α and β are stress level parameters; R is the molar gas constant taken as 8.31 $J\cdot mol^{-1}\cdot K^{-1}$; T is the absolute temperature (K); Q is thermal deforming activation energy ($kJ\cdot mol^{-1}$).

For the hyperbolic sine function $\sinh\left(x\right)=\left(e^{x}-e^{-x}\right)/2$, that's Taylor's expansion, as expressed in Equation 2.

$$\sinh\left(x\right)=\frac{e^{x}-e^{-x}}{2}=x+\frac{x^3}{3!}+\frac{x^5}{5!}+\frac{x^7}{7!}+\cdots\cdots \tag{2}$$

When $x \le 0.8$, the relative error is less than 4.2% when more than three-degree terms are ignored; When $x \ge 1.2$, the relative error is less than 1.9% when e^{-x} are ignored[15]. Then, the hyperbolic-sine Arrhenius-type constitutive equation can be simplified as Equation 3. where $\alpha = \beta / C$.

$$\left.\begin{array}{ll} \dot{\varepsilon} = A_1\sigma_P{}^{C} exp\left[-Q/\left(RT\right)\right] & \alpha\sigma < 0.8 \\ \dot{\varepsilon} = A_2 exp\left(\beta\sigma_P\right) exp\left[-Q/\left(RT\right)\right] & \alpha\sigma > 1.2 \\ \dot{\varepsilon} = A\left[\sinh\left(\alpha\sigma_P\right)\right]^n exp\left[-Q/\left(RT\right)\right] & for\ all\ \sigma \end{array}\right\} \tag{3}$$

In order to obtain the parameters in Equation 3. Taking the natural logarithm on both sides of Equation 3 gives.

$$\left.\begin{array}{ll} ln\dot{\varepsilon} = \ln A_1 + C ln\sigma_P - Q/\left(RT\right) & \alpha\sigma < 0.8 \\ ln\dot{\varepsilon} = \ln A_2 + \beta\sigma_P - Q/\left(RT\right) & \alpha\sigma > 1.2 \end{array}\right\} \tag{4}$$

$$\ln\dot{\varepsilon} = \ln A + n\ln\left[\sinh\left(\alpha\sigma_P\right)\right] - Q/\left(RT\right) \quad \text{for all}\,\sigma \tag{5}$$

From Equation 4, it can be derived that $C = \partial\left(\ln\dot{\varepsilon}\right)/\partial\left(\ln\sigma_P\right)$, and $\beta = \partial\left(\ln\dot{\varepsilon}\right)/\partial\left(\sigma_P\right)$. The relationships of $\ln\dot{\varepsilon}$ versus $\ln\sigma_P$, and $\ln\dot{\varepsilon}$ versus σ_P under different deformation temperatures were fitted linearly as Figure 4a and 4b. The slopes of curves in Figure 4a and 4b are the values of C and β. Then, the average values of C and β can be obtained as 4.4431, and 0.0315 Mpa^{-1}, respectively. Thus, $\alpha = \beta / C = 0.0071$. By substituting the values of peak stresses, strain rates and α into Equation 5, the relationships of $\ln\dot{\varepsilon}$ versus $\ln\left[\sinh\left(\alpha\sigma_P\right)\right]$ can be obtained, as shown in Figure 5a. Then, the average values of n can be calculated as 2.8702.

Similarly, the relationships of $1/T$ versus $\ln\left[\sinh\left(\alpha\sigma_P\right)\right]$ under different strain rates were fitted linearly as Figure 5b. Then, the average values of material constants Q and A can be obtained as 371.946 $kJ\cdot mol^{-1}$ and 2.2957×10^{13}, respectively.

According to Zener and Hollomon[16], the Zener-Hollomon parameter was introduced to describe the combined influence of strain rate and temperature on flow stress, and their correlation can be described as Equation 6. The relationships of $\ln Z$

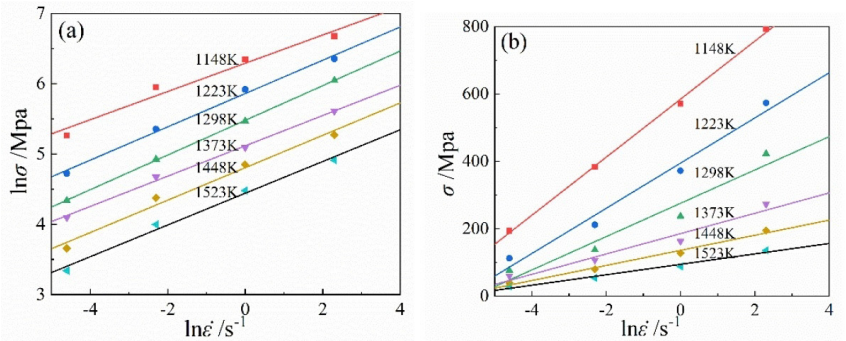

Figure 4. Relationships between strain rates and peak stresses: (a) $\ln\dot{\varepsilon}$ versus $\ln\sigma_P$; (b) $\ln\dot{\varepsilon}$ versus σ_P.

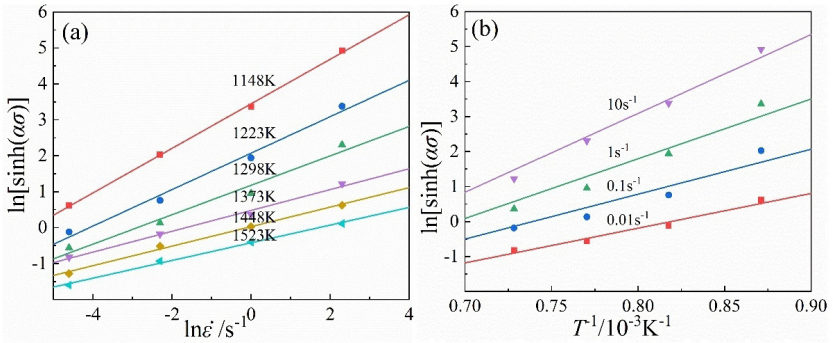

Figure 5. Relationships between: (a) $1/T$ versus $\ln\left[\sinh\left(\alpha\sigma_P\right)\right]$; (b) $\ln\dot{\varepsilon}$ versus $\ln\left[\sinh\left(\alpha\sigma_P\right)\right]$.

versus $\ln\left[\sinh\left(\alpha\sigma_{\mathrm{P}}\right)\right]$ under different strain rates were fitted linearly as Figure 6a. Combining Equation 1 and Equation 6, the peak flow stress can be derived as Equation 7.

$$Z=\dot{\varepsilon}\exp\left[Q/RT\right]=A[\sinh\left(\alpha\sigma\right)]^{n} \tag{6}$$

$$\sigma_{\mathrm{P}}=\frac{1}{\alpha}\ln\left\{\left(\frac{Z}{A}\right)^{1/n}+\left[\left(\frac{Z}{A}\right)^{2/n}+1\right]^{1/2}\right\} \tag{7}$$

Meanwhile, the peak strain strongly depends on the deformation temperature and strain rate, and the relationships generally can be expressed as the following function:

$$\varepsilon_{\mathrm{p}}=kZ^{m} \tag{8}$$

Where k and m are material constants, taking the natural logarithm on both sides of Equation 8 gives.

$$\ln\varepsilon_{\mathrm{p}}=m\ln Z+\ln k \tag{9}$$

The values of m and k can be obtained from the slope and intercept of the linear fitting line in the $\ln\varepsilon_{\mathrm{p}}-\ln Z$ plot (Figure 6b) as 0.0854 and 0.0046, respectively.

Substituting the values of α, n and A into Equation 7, the value of Q into Equation 6, the value of m and k into Equation 9, the Arrhenius-type constitutive equation for Ni-38Cr-3.8Al alloy at peak stress can be obtained as the following equations.

$$\begin{cases}\sigma_{\mathrm{P}}=\dfrac{1}{0.0071}\ln\left\{\left(\dfrac{Z}{2.2957\times10^{13}}\right)^{1/2.8702}+\left[\left(\dfrac{Z}{2.2957\times10^{13}}\right)^{2/2.8702}+1\right]^{1/2}\right\}\\ \varepsilon_{\mathrm{p}}=0.0046\times Z^{0.0854}\\ Z=\dot{\varepsilon}\exp\left[\dfrac{371.946}{RT}\right]\end{cases} \tag{10}$$

It is well-accepted that the strain also has a great influence on thermal deformation behaviors and flow stress evolution of alloys. In this work, in order to preciously describe the flow behaviors of Ni-38Cr-3.8Al alloy, the solved constitutive equation at peak stress was modified by considering the effect of strain on flow stress.

The polynomial function was used to fit the relationships between strain and variable coefficients including Q, n, A and α, as expressed in Equation 11 and Equation 12. The fitted results in the strain range of 0~0.9 with 0.1 intervals were depicted in Figure 7. And the solved coefficients for polynomial functions of $Q(\varepsilon)$, $n(\varepsilon)$, $\ln A(\varepsilon)$ and $\alpha(\varepsilon)$ were listed in Table 1.

$$\begin{cases}\alpha(\varepsilon)=B_0+B_1\varepsilon+B_2\varepsilon^2+B_3\varepsilon^3+B_4\varepsilon^4+B_5\varepsilon^5\\ \ln A(\varepsilon)=C_0+C_1\varepsilon+C_2\varepsilon^2+C_3\varepsilon^3+C_4\varepsilon^4+C_5\varepsilon^5\\ n(\varepsilon)=D_0+D_1\varepsilon+D_2\varepsilon^2+D_3\varepsilon^3+D_4\varepsilon^4+D_5\varepsilon^5\\ Q(\varepsilon)=E_0+E_1\varepsilon+E_2\varepsilon^2+E_3\varepsilon^3+E_4\varepsilon^4+E_5\varepsilon^5\end{cases} \tag{11}$$

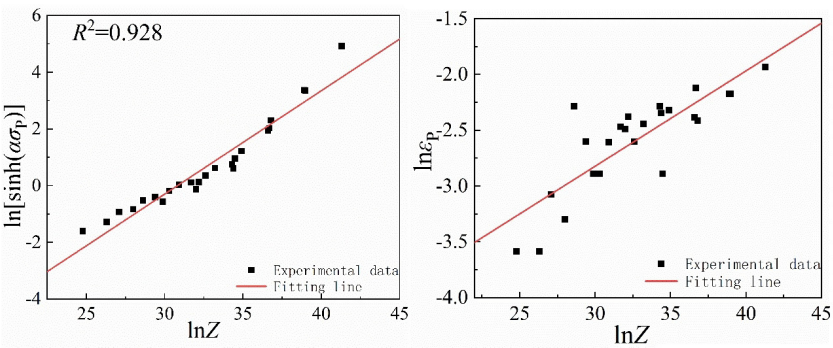

(a) (b)

Figure 6. Relationship between: (a) the peak stress and Zener-Hollomon parameter; (b) the peak strain and Zener-Hollomon parameter.

Table 1. Solved coefficients for polynomial functions of $Q(\varepsilon)$, $n(\varepsilon)$, $\ln A(\varepsilon)$ and $\alpha(\varepsilon)$.

	α(ε) (B_i)	ln$A$(ε) (C_i)	$n(\varepsilon)$ (D_i)	$Q(\varepsilon)$ (E_i)
Typical	0.00743	29.6	2.54	358.2
	0.00019	38.6	5.93	442.3
	-0.0131	-306.4	-32.5	-3551.5
	0.0635	742.5	86.1	8680.4
	-0.0915	-786.9	-99.2	-9267.2
	0.0431	309.2	42.29	3664.6

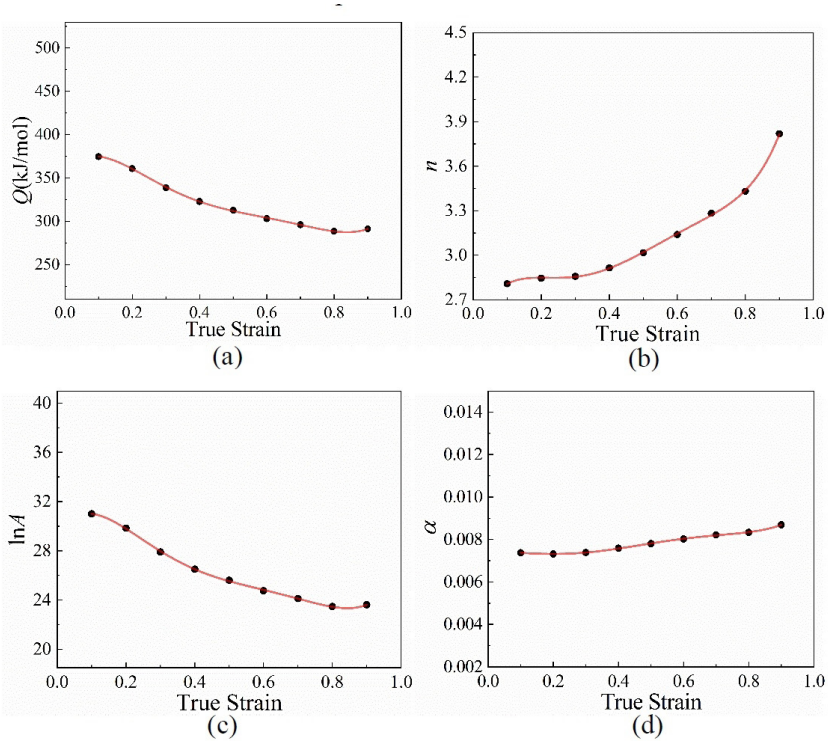

Figure 7. Relationships between strain and variable coefficients: (a) Q; (b) n; (c) ln$A$; (d) α.

Table 2. The values of α, n, ln$A$ and Q under different temperatures.

Temperatures	α	n	ln$A$	Q
1148 K	0.002332	1.6137	29.1055	211.8164
1223 K	0.003532	1.9719	30.6540	259.9235
1298 K	0.004986	2.4424	31.1042	317.9193
1373 K	0.007141	3.4476	31.2285	458.7464
1448 K	0.010292	3.6831	30.8337	443.9784
1523 K	0.014573	4.0624	30.6004	555.4782
Average values	0.00709131	2.8702	30.7647	371.946
Standard deviation (s)	0.004202356	0.9114	0.6999	120.7427
Coefficient of variation (COV)	59.3%	31.8%	2.3%	32.2%

Finally, substituting the polynomial functions of $Q(\varepsilon)$, $n(\varepsilon)$, ln$A(\varepsilon)$ and $\alpha(\varepsilon)$ into Equation 10, the modified Arrhenius constitutive equation with compensation of strain for Ni-38Cr-3.8Al alloy can be obtained as follows.

$$\sigma=\frac{1}{\alpha(\varepsilon)}\ln\left\{\left(\frac{\dot{\varepsilon}\exp\left[Q(\varepsilon)/8.31T\right]}{A(\varepsilon)}\right)^{1/n(\varepsilon)}+\left[\left(\frac{\dot{\varepsilon}\exp\left[Q(\varepsilon)/8.31T\right]}{A(\varepsilon)}\right)^{2/n(\varepsilon)}+1\right]^{\frac{1}{2}}\right\} \tag{12}$$

3.3. Solving process of improved Arrhenius-type constitutive equation

For phenomenological constitutive equations, there will inevitably exist errors with the experimental value in the fitting process of material constants. With the accumulation of fitting errors, the accuracy of the constitutive equation decreases gradually so that may not satisfy the requirement of numerical simulation. In order to further evaluate the reliability of the constitutive equation, the standard deviation (s) and coefficient of variation (COV) were employed. The calculation methods can be described as Equation 13 and Equation 14, respectively. The values of s and COV for material constants (α, n, ln$A$ and Q) under different temperatures are listed in Table 2.

$$s=\frac{\sum_{i=1}^{N}\left(x_i-\bar{x}\right)^2}{N-1} \tag{13}$$

$$COV(\%)=\frac{s}{\bar{x}}\times 100\% \tag{14}$$

where x is the value of material constants including α, n, ln$A$ and Q under different temperatures, respectively; N is the number of statistical samples.

As can be seen from Table 2, the value distributions of material constants α, n and Q are relatively discrete, with COV of variation reaching 59.3%, 31.8% and 32.2%, respectively. This is because in the process of hot working, the rise of temperature will affect the evolution of material microstructure (such as phase transition), thus affecting the deformation resistance of the material, and eventually leading to the dispersion of peak stress distribution. It can be seen from Figure 2 that in the hot deformation process of Ni-38Cr-3.8Al alloy, the DRX-type curves and DRV-type curves appear at lower temperatures of 1148 K, 1223 K and 1298 K, and higher temperatures of 1373 K, 1448 K and 1523 K, respectively. Meanwhile, as indicated in the work of McQueen et al.[14], the stress multiplier α is an additional adjustable constant which brings the $\alpha\sigma$ into the correct range. Therefore, in order to accurately describe the flow behaviors of Ni-38Cr-3.8Al alloy, taking the temperature of 1298K as the segmented point, a segmented Arrhenius-type constitutive equation was developed.

By the similar method shown in Section 3.2, by substituting the peak stress and strain rates at lower temperatures into Equation 4 and Equation 5, the average values of C and β can be obtained as 4.418, and 0.0156 Mpa^{-1}, respectively and $\alpha = \beta / C = 0.0035$. Thus, the average value of n can be calculated as 3.1452. Then, the average values of material constants Q and A can be obtained as 377.7278 kJ·mol^{-1} and 1.1065×10^{13}, respectively. Similarly, the values of material constants at higher temperatures can be calculated by linear fitting. Finally, the values of s and COV for material constants (α, n, ln$A$ and Q) under different temperatures were listed in Table 3. Compare with before segmenting, the COV of material constants α, n and Q after segmenting has a significant decline, and the value is 29%, 8.9% and 9.4%, respectively. This indicates that the error generated in the fitting process can be reduced by using temperature interval prediction.

The relationships of $\ln\left[\sinh\left(\alpha\sigma_P\right)\right]$ versus $\ln Z$ were fitted linearly as Figure 8a. It is found that the coefficient of determination R^2 of the improved constitutive equation is higher than that of the typical. The relationships of $\ln\varepsilon_P$ versus $\ln Z$ were fitted linearly as Figure 8b, where the slope

Table 3. The values of α, n, ln$A$ and Q under different temperatures.

Temperatures		α	n	ln$A$	Q
$T \le 1298$K	1148 K	0.0023321	2.91	29.86	299.9738
	1223 K	0.0035322	3.12	30.17	321.8648
	1298 K	0.0049857	3.41	30.04	351.5482
	Average values	0.003617	3.15	30.02	324.4623
	s	0.001085	0.205	0.125	21.1351
	COV	30%	6.5%	0.4%	6.5%
>1298K	1373 K	0.0071407	2.73	29.19	322.2579
	1448 K	0.0102921	3.16	29.36	372.4961
	1523 K	0.0145728	3.7	29.55	437.0808
	Average values	0.010669	3.2	29.37	377.2783
	s	0.003046	0.356772	0.144963	46.998
	COV	28.5%	11.2%	0.5%	12.5%
Average s		0.004202	0.9114	0.6999	120.7427
Average COV		29.3%	8.8%	0.45%	9.4%

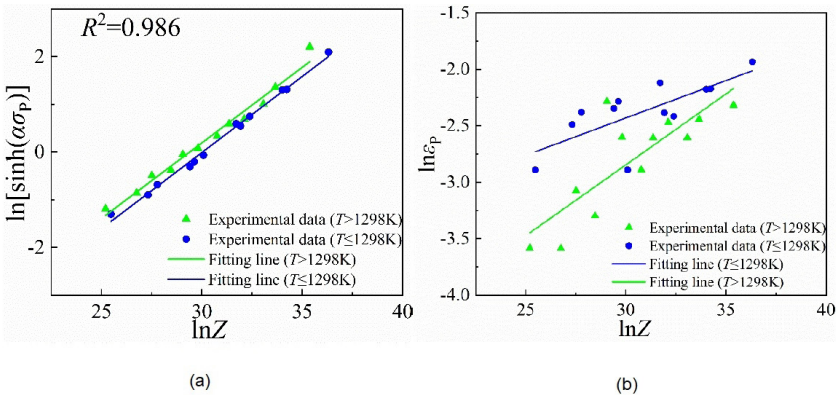

Figure 8. Relationship between: (a) the peak stress and Zener-Hollomon parameter; (b) the peak strain and Zener-Hollomon parameter.

and intercept of the straight line offer the values of m and $\ln k$, respectively. It can be seen that the calculated material constants $m = 0.0662$ and $k = 0.0121$.

Substituting the values of α, n and A into Equation 7, the value of Q into Equation 6, the value of m and k into Equation 9, the improved constitutive equation for Ni-38Cr-3.8Al alloy at peak stress can be obtained as the following equations.

$$\sigma_P = \begin{cases} \dfrac{1}{0.0035}\ln\left\{\left(\dfrac{Z}{1.1065\times10^{13}}\right)^{\frac{1}{3.1452}} + \left[\left(\dfrac{Z}{1.1065\times10^{13}}\right)^{\frac{2}{3.1452}}+1\right]^{1/2}\right\} & (T \le 1298\,\mathrm{K}) \\ \dfrac{1}{0.0106}\ln\left\{\left(\dfrac{Z}{5.7348\times10^{12}}\right)^{\frac{1}{3.1973}} + \left[\left(\dfrac{Z}{5.7348\times10^{12}}\right)^{\frac{2}{3.1973}}+1\right]^{1/2}\right\} & (T > 1298\,\mathrm{K}) \end{cases} \quad (15)$$

$$\varepsilon_P = \begin{cases} 0.0121\times Z^{0.0662} & (T \le 1298\,\mathrm{K}) \\ 0.0013\times Z^{0.1256} & (T > 1298\,\mathrm{K}) \end{cases}$$

$$Z = \begin{cases} \dot{\varepsilon}\exp\left[\dfrac{377.7278}{RT}\right] & (T \le 1298\,\mathrm{K}) \\ \dot{\varepsilon}\exp\left[\dfrac{324.4623}{RT}\right] & (T > 1298\,\mathrm{K}) \end{cases}$$

Considering the effect of strain on flow stress, the variable coefficients including Q, n, A and α are regarded as polynomial functions of strain, as expressed in Equation 11 and Equation 12. The fitted results of improved Arrhenius-type constitutive equation in the strain range of 0~0.9 with 0.1 intervals were depicted in Figure 9. And the solved coefficients for polynomial functions of $Q(\varepsilon)$, $n(\varepsilon)$, $\ln A(\varepsilon)$ and $\alpha(\varepsilon)$ were listed in Table 4.

Finally, substituting the polynomial functions of $Q(\varepsilon)$, $n(\varepsilon)$, $\ln A(\varepsilon)$ and $\alpha(\varepsilon)$ into Equation 11, the modified Arrhenius constitutive equation at higher temperatures and lower temperatures for Ni-38Cr-3.8Al alloy can be obtained, respectively.

3.4. Comparisons of the typical and improved Arrhenius-type constitutive equations

In order to evaluate the predictive ability of the modified Arrhenius-type constitutive equations of Ni-38Cr-3.8Al alloy, the comparisons of flow stress between experimental results and predicted ones have been done. The predicted stress values of typical and improved Arrhenius-type constitutive equations in the strain range of 0~0.9 with 0.1 intervals are calculated according to the constitutive equations in Equation 12. Figure 10 and Figure 11 show the comparison results of flow stress between the experiment and predicted by the typical and improved constitutive equations at different deformation conditions, respectively. It is apparently found that the stress variation trend, which is

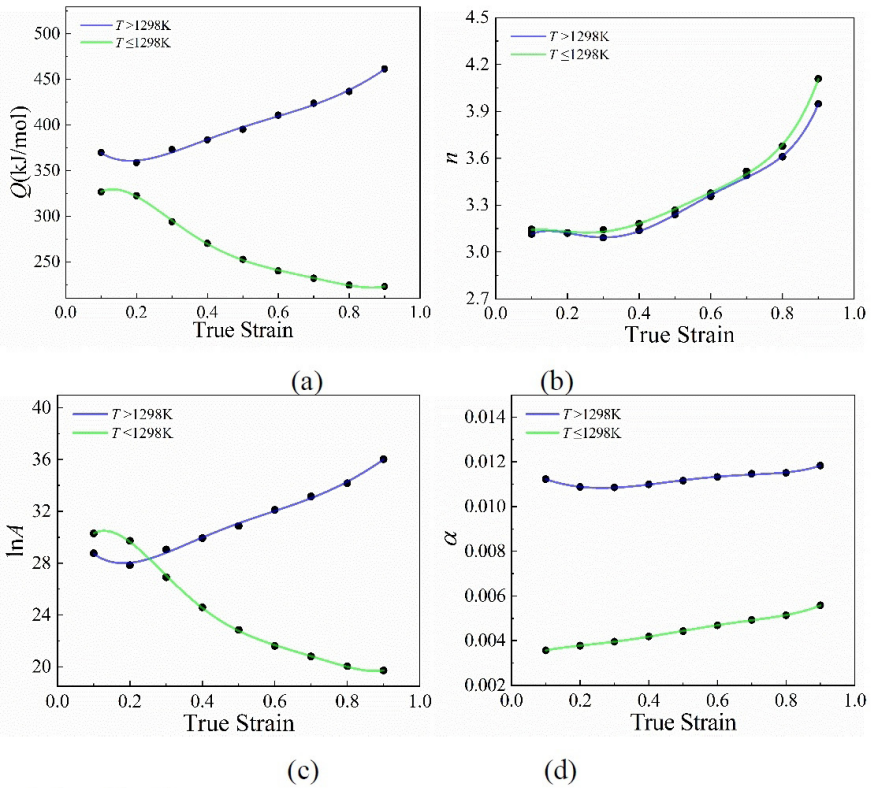

Figure 9. Relationships between strain and variable coefficients: (a) Q; (b) n; (c) $\ln A$; (d) α.

Table 4. Solved coefficients for polynomial functions of $Q(\varepsilon)$, $n(\varepsilon)$, $\ln A(\varepsilon)$ and $\alpha(\varepsilon)$ in the improved equations.

Temperature	$\alpha(\varepsilon)$ (Bi)	$\ln A(\varepsilon)$ (C_i)	$n(\varepsilon)$ (D_i)	$Q(\varepsilon)$ (E_i)
T ≤ 1298K	0.00309	25.3	3.12	269.8
	0.0074	96.98	2.44	1079.5
	-0.0341	-577.6	-18.1	-6308.9
	0.0916	1226.1	55.1	13417.5
	-0.1079	-1165.7	-68.9	-12833.5
	0.0463	416.6	31.6	4624.5
T > 1298K	0.01196	32.7	2.81	415.8
	0.00941	-64.9	5.97	-747.7
	0.0212	299.4	-38.1	3390.2
	0.00239	-547.7	101.9	-6045.1
	0.0402	463.5	-116.6	4964.1
	0.0267	-144.91	48.8	-1486.8

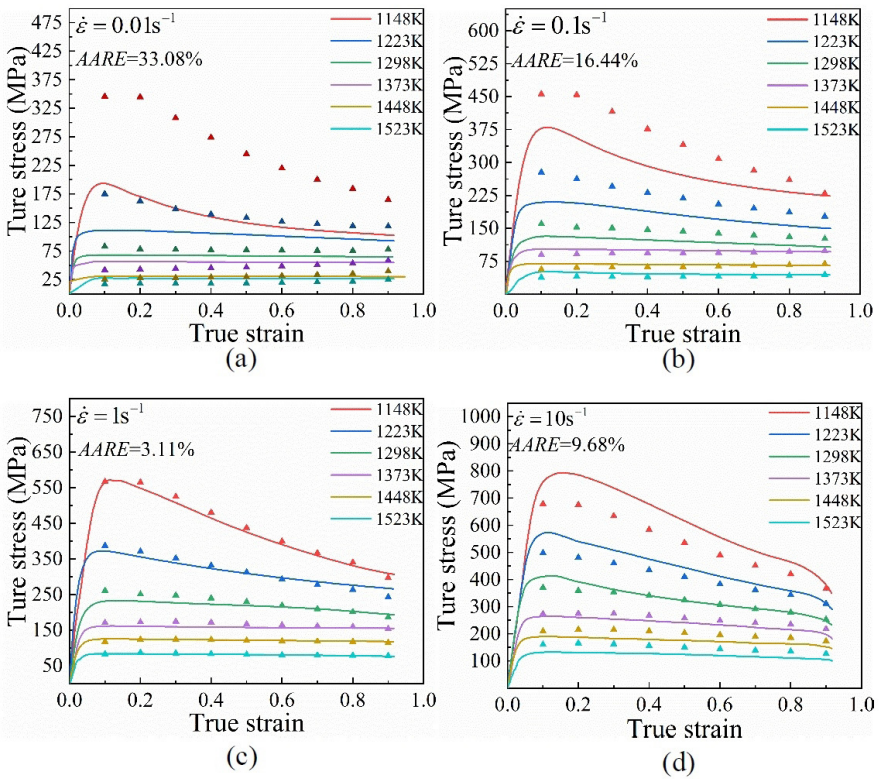

Figure 10. The predicted stress values of the typical constitutive equation and experimental stress-stain curves of Ni-38Cr-3.8Al alloy under strain rates of: (a) 0.01 s^{-1}; (b) 0.1 s^{-1}; (c) 1 s^{-1}; (d) 10 s^{-1}.

predicted by typical and improved constitutive equations, is consistent with the experimental stress-strain curves. There is a significant difference between the predicted stress values of the typical and improved constitutive equations under all temperature conditions. As shown in Figure 10, at strain rates of 0.01 s^{-1} and 0.1 s^{-1}, the predicted stress values of the typical equation are much higher than the experimental value at lower temperatures and slightly lower than the experimental value at higher temperatures, and the *AARE*-values were calculated as 33.08% and 16.44%, respectively. In contrast, at strain rates of 10 s^{-1}, the predicted stress values of the typical equation are lower than the experimental value at lower temperatures and slightly lower than the experimental value at higher temperatures, and the *AARE*-

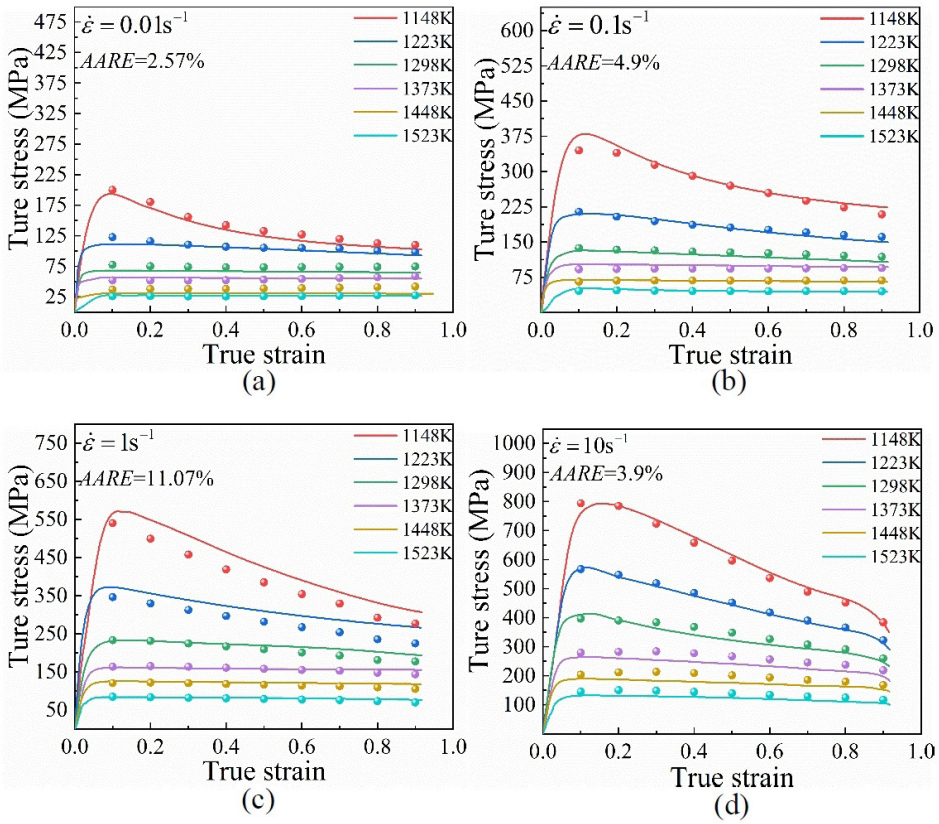

Figure 11. The predicted stress values of improved constitutive equation and experimental stress-stain curves of Ni-38Cr-3.8Al alloy under strain rates of: (a) 0.01 s^{-1}; (b) 0.1 s^{-1}; (c) 1 s^{-1}; (d) 10 s^{-1}.

value was calculated as 9.68%. Meanwhile, at strain rates of 1 s^{-1}, the predicted stress values of the typical equation have a good agreement with the experimental values, and the *AARE*-value was calculated at only 3.11%. This is due to the distribution of experimental stress values and material constants at a certain strain being relatively discrete, the large fitting errors in the solving process of Arrhenius-type constitutive equation will generate. According to Xia et al.[13], the stress multiplier α is an additional adjustable constant that brings the predicted stress values into the correct range. By segmenting stress-strain curves into DRX-type curves and DRV-type curves based on the temperature of 1298K, the *COV* of material constant α has declined from 59.3% to 29%. This means that the errors generated in the process of linear fitting of material constants will be greatly reduced. Combining Figure 10 and Figure 11, it can be seen that the predicted stress values have a good agreement with the experimental values by establishing constitutive equations at lower and higher temperatures, respectively. The *AARE*-values at strain rates of 0.01 s^{-1}, 0.1 s^{-1}, 1 s^{-1} and 10 s^{-1} were calculated as 2.57%, 4.9%, 11.07% and 3.9%. In conclusion, for Ni-38Cr-3.8Al alloy, the predicted stress values of the improved Arrhenius constitutive equation have a greater agreement with the experimental stress-strain curves than the typical Arrhenius constitutive equation.

In the work of Quan et al.[17] and Rudra et al.[18], the *AARE* was employed to evaluate the precision for SAE 5137H alloy and aluminum 5083+10 wt pct SiC_p particulate composite, respectively, and their *AARE*-values were calculated as 7.3% and 4.621% respectively. To further evaluate the prediction accuracy of the constitutive model, the error between predicted results and experimental ones was calculated. The correlation coefficient (*R*) and average absolute relative error (*AARE*) were employed for a comprehensive evaluation, and their calculation methods can be described as Equation 16 and Equation 17, respectively.

$$R = \frac{\sum_{i=1}^{N}\left(\sigma_{EM_i} - \overline{\sigma_{EM}}\right)\left(\sigma_{PR_i} - \overline{\sigma_{PR}}\right)}{\sqrt{\sum_{i=1}^{N}\left(\sigma_{EM_i} - \overline{\sigma_{EM}}\right)^2\left(\sigma_{PR_i} - \overline{\sigma_{PR}}\right)^2}} \tag{16}$$

$$AARE(\%) = \frac{1}{N}\sum_{i=1}^{N}\left|\frac{\sigma_{EM_i} - \sigma_{PR_i}}{\sigma_{EM_i}}\right| \times 100\% \tag{17}$$

where σ_{EM} and σ_{PR} are the experimental flow stress and predicted flow stress, respectively. *N* is the number of statistical samples. Figure 12 shows the relationship of predicted and experimental flow stress. Here, the *R* and *AARE* values of the typical and improved constitutive equations considered strain compensation were calculated as 0.932, 15.83% and 0.9963, 5.61%, respectively. Compared with the work of

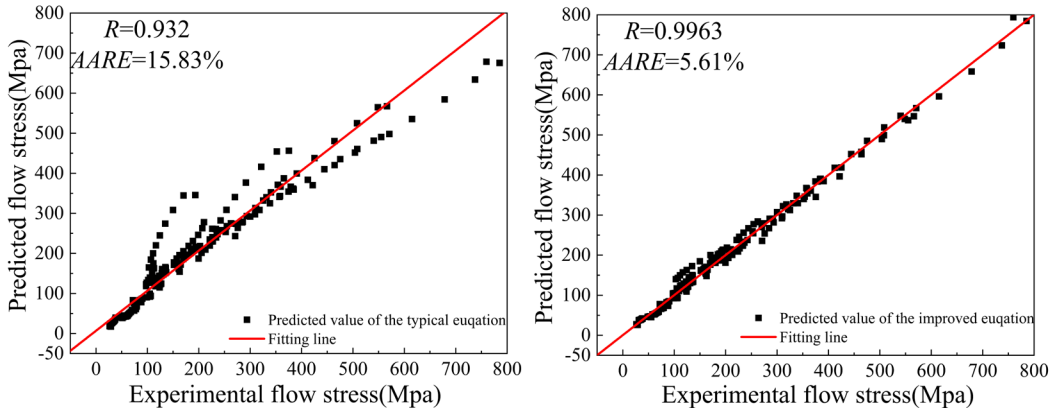

Figure 12. Relationship of the typical and improved constitutive equation predicted and experimental flow stress.

Quan et al.[17] and Rudra et al.[18], the *AARE* value of typical constitutive equation is so large that cannot describe the flow behavior of the material accurately. For the phenomenological constitutive equation, it is acceptable that the *AARE*-value of improved constitutive equations is only 5.61%. Therefore, the improved Arrhenius constitutive equations have a larger *R*-value and lower *AARE*-value, which indicates that the improved constitutive equation has superior rationality and correlation than the typical constitutive equation.

4. Conclusions

The thermal deformation behaviors of Ni-38Cr-3.8Al alloy were characterized based on the isothermal compression experiments at the strain rate range of 0.01~10 s^{-1} and temperature range of 1148~1523 K. To further accurately and efficiently describe the complex flow behaviors of this alloy, a typical and an improved segmented Arrhenius-type constitutive model were established according to the obtained stress-strain data. The following main conclusions were acquired from the current study.

(1) The true stress-strain curves of Ni-38Cr-3.8Al alloy exhibit the typical characteristics of DRX and DRV softening behaviors. Specifically, the DRX-type curves and DRV-type curves manifest at lower temperatures of 1148 K, 1223 K and 1298 K, and higher temperatures of 1373 K, 1448 K and 1523 K, respectively. Furthermore, the flow stress exhibits a decreasing trend with temperature increasing and strain rate decreasing.

(2) An improved segmented Arrhenius-type constitutive model, considering the softening characteristics of DRX and DRV at different temperatures, was developed to accurately describe the complicated relationships between flow stress and processing parameters. In this model, the activation energy Q, structure factor A, stress exponent n, and stress parameters α were fitted as the polynomial functions of true strain.

(3) Two indicators, R and *AARE,* were employed to evaluate the prediction accuracy of the constitutive model, and their values were calculated as 0.932, 15.83% and 0.9963, 5.61% for the typical and improved constitutive equations, respectively. It indicates that the improved Arrhenius-type constitutive model is effective in predicting the thermal deformation behaviors of Ni-38Cr-3.8Al alloy.

5. Acknowledgments

The authors are grateful for the supports from National Natural Science Foundation of China (52175287), and Chongqing Natural Science Foundation General Project (CSTB2022NSCQ-MSX0593).

6. References

1. Koyanagi Y, Takabayashi H, Yasuda HY. Influence of Cr content on cellular precipitation behaviour of Ni-38Cr-3.8Al alloy with lamellar structure. Mater Sci Forum. 2018;941:1203-9.
2. Ueta S, Kajihara M. Influence of Al on kinetics of discontinuous precipitation in Ni-38Cr alloy. ISIJ Int. 2010;50(11):1676-82.
3. Koyanagi Y, Takabayashi H, Ueta S, Cho K, Yasuda HY. Creep behavior of Ni-38Cr-3.8Al alloy with lamellar structure formed by discontinuous precipitation. Mater Sci Eng A. 2019;766:138333.
4. Takahata N, Ueta S, Shimizu T. Influence of heat treatment on microstructure and hardness of Ni-Cr-Al alloy. Denki-Seiko. 2004;75:97-105.
5. Ueta S. Material properties of high hardness and high corrosion resistant Ni-based alloy "DSA760". Denki-Seiko. 2012;83:69-73.
6. Sellars CM, McTegart WJ. On the mechanism of hot deformation. Acta Metall. 1966;14(9):1136-8.
7. Song SX, Horton JA, Kim NJ, Nieh TG. Deformation behavior of a twin-roll-cast Mg-6Zn-0.5Mn-0.3Cu-0.02Zr alloy at intermediate temperatures. Scr Mater. 2007;56(5):393-5.
8. Cingara A, McQueen HJ. New method for determining sinh constitutive constants for high temperature deformation of 300 austenitic steels. J Mater Process Technol. 1992;36(1):17-30.
9. Lin YC, Chen M-S, Zhong J. Constitutive modeling for elevated temperature flow behavior of 42CrMo steel. Comput Mater Sci. 2008;42(3):470-7.
10. Nie Y, Zheng J, Han R, Jia L, Zhang Z, Xue Y. Hot deformation behaviour and constitutive equation of Mg-9Gd-4Y-2Zn-0.5Zr alloy. Materials. 2022;15(5):1779.
11. Quan G, Shi Y, Yu C, Zhou J. The improved arrhenius model with variable parameters of flow behavior characterizing for the as-cast AZ80 magnesium alloy. Mater Res. 2013;16(4):785-91.
12. Yi S-X, Yang Z-J, Xie H-X. Hot deformation and constitutive modeling of TC21 titanium alloy. Materials. 2022;15(5):1923.
13. Xia YF, Jiang W, Cheng Q, Jiang L, Jin L. Hot deformation behavior of Ti-6Al-4V-0.1Ru alloy during isothermal compression. Trans Nonferrous Met Soc China. 2020;30(1):134-46.

14. McQueen HJ, Ryan ND. Constitutive analysis in hot working. Mater Sci Eng A. 2002;322(1-2):43-63.
15. McQueen HJ, Yue S, Ryan ND, Fry E. Hot working characteristics of steels in austenitic state. J Mater Process Technol. 1995;53(1-2):293-310.
16. Zener C, Hollomon H. Effect of strain rate upon plastic flow of steel. J Appl Phys. 1944;15(1):22-32.
17. Quan G, Zhang Y, Lei S, Xiong W. Characterization of flow behaviors by a PSO-BP integrated model for a medium carbon alloy steel. Materials. 2023;16(8):2982.
18. Rudra A, Ashiq M, Das S, Dasgupta R. Constitutive modeling for predicting high-temperature flow behavior in aluminum 5083+10 Wt Pct SiC_p composite. Metall Mater Trans, B, Process Metall Mater Proc Sci. 2019;50(2):1060-76.